Exploration of Targeted Anti-tumor Therapy

Open Exploration

Open Access Original Article

Engineering S3 domain-fused octameric methionine γ-lyase for enhanced therapeutic methionine depletion in cancer

Louay Abo Qoura[1,2,3*], Ayman Younes[1], Nikolay A. Bondarev[4], Maria M. Buben[4], Ilya V. Manukhov[4], Vadim S. Pokrovsky[1,2*]

[1]Department of Biochemistry, Research Institute of Molecular and Cellular Medicine, People's Friendship University of Russia (RUDN University), 117198 Moscow, Russia

[2]N.N. Blokhin National Medical Research Center of Oncology, Ministry of Health of the Russian Federation, 115478 Moscow, Russia

[3]Russian Gerontology Clinical Research Centre, Pirogov Russian National Research Medical University, 129226 Moscow, Russia

[4]Moscow Institute of Physics and Technology, 141700 Dolgoprudny, Russia

***Correspondence:** Louay Abo Qoura, Department of Biochemistry, Research Institute of Molecular and Cellular Medicine, People's Friendship University of Russia (RUDN University), 117198 Moscow, Russia. louay.ko@gmail.com; Vadim S. Pokrovsky, N.N. Blokhin National Medical Research Center of Oncology, Ministry of Health of the Russian Federation, 115478 Moscow, Russia. v.pokrovsky@ronc.ru

Academic Editor: Nicola Normanno, Fondazione Policlinico Universitario Agostino Gemelli IRCCS, Italy

Received: April 15, 2026 **Accepted:** September 4, 2026 **Published:** November 22, 2026

Cite this article: Abo Qoura L, Younes A, Bondarev NA, Buben MM, Manukhov IV, Pokrovsky VS. Engineering S3 domain-fused octameric methionine γ-lyase for enhanced therapeutic methionine depletion in cancer. Explor Target Antitumor Ther. 2026;7:1002414. https://doi.org/10.37349/etat.2026.1002414

Abstract

Aim: Methionine depletion represents a promising therapeutic strategy for methionine-dependent malignancies, although the clinical translation of recombinant methionine γ-lyase (rMGL) remains constrained by a short circulating half-life and insufficient tumor localization. A previously engineered epidermal growth factor receptor-targeting S3 domain-fused octameric methionine γ-lyase was comprehensively evaluated to determine whether receptor-directed localization enhances biological activity and therapeutic efficacy across complementary preclinical cancer models.

Methods: The cytotoxic activities of rMGL and its engineered variant (rMGL-S3) were evaluated across a panel of human cancer cell lines, including HCT116, DU145, PC3, MCF7, MDA-MB-231, Panc1, and MIA PaCa-2, under continuous exposure and enzyme washout conditions in vitro. Cell-cycle perturbations were analyzed by flow cytometry in epidermal growth factor receptor-overexpressing cell models. Therapeutic efficacy and tolerability were subsequently evaluated in A431, HCT116, and Panc1 xenograft models following intraperitoneal and intravenous administration, with direct comparison to the parental recombinant enzyme.

Results: rMGL-S3 preserved potent cytotoxic activity following the removal of unbound enzyme, whereas the parental enzyme completely lost measurable activity under identical experimental conditions, supporting prolonged tumor-associated functional retention. Distinct cell-cycle perturbations were observed across different tumor models, indicating context-dependent responses to methionine

© The Author(s) 2026. This is an Open Access article licensed under a Creative Commons Attribution 4.0 International License (https://creativecommons.org/licenses/by/4.0/), which permits unrestricted use, sharing, adaptation, distribution and reproduction in any medium or format, for any purpose, even commercially, as long as you give appropriate credit to the original author(s) and the source, provide a link to the Creative Commons license, and indicate if changes were made.

deprivation. Superior antitumor efficacy was consistently demonstrated in vivo, achieving tumor growth inhibition of 56% (p = 0.032) in A431, 45% (p = 0.029) in HCT116, and 36% (p = 0.05) in Panc1 xenografts while maintaining favorable tolerability without detectable systemic toxicity.

Conclusions: Comprehensive preclinical validation demonstrates that receptor-directed localization substantially augments the therapeutic performance of S3 domain-fused methionine γ-lyase. Integration of molecular targeting with enzymatic methionine restriction establishes a rational strategy for improving tumor-selective amino acid deprivation therapy and provides a strong translational foundation for the further clinical development of targeted metabolic therapeutics.

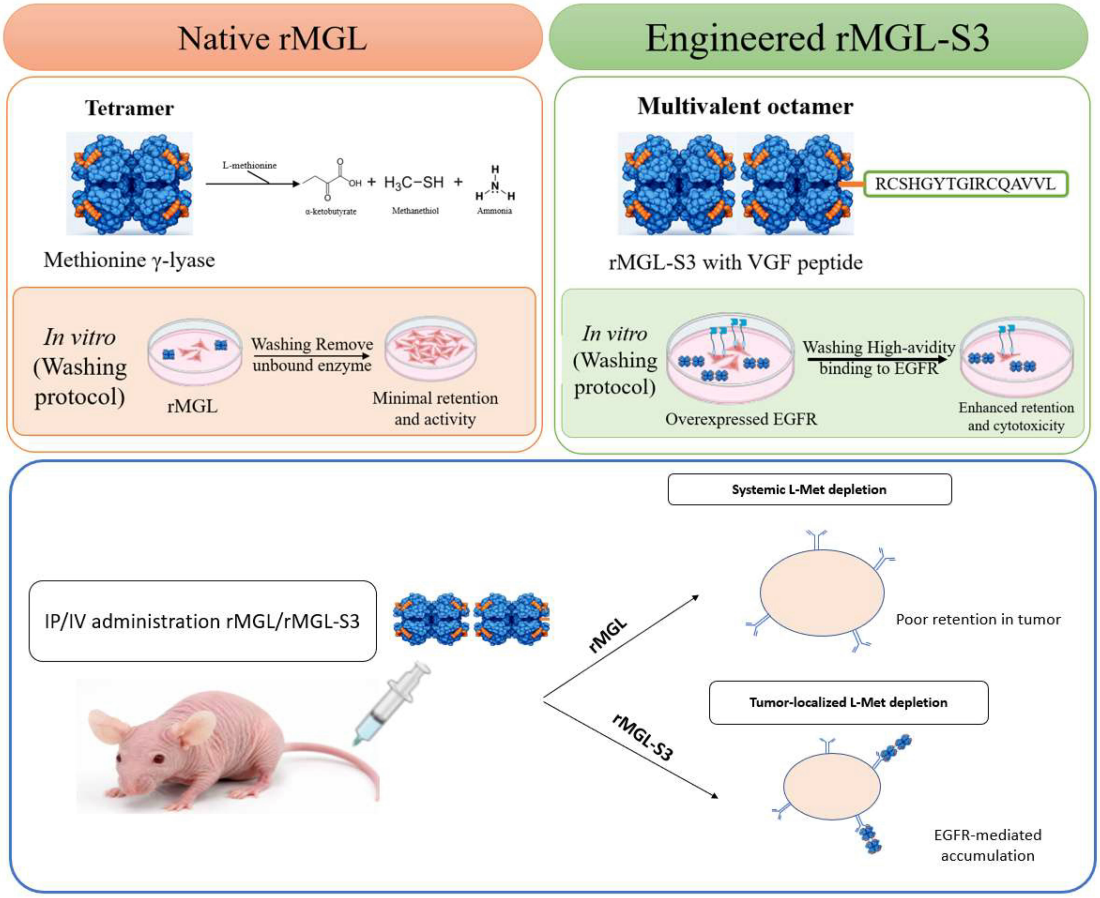

Graphical abstract. EGFR-targeted engineering improves tumor-associated retention and antitumor activity of methionine γ-lyase. VGF: vaccinia growth factor; EGFR: epidermal growth factor receptor; IP: intraperitoneal; IV: intravenous.

Keywords

methioninase, methionine deprivation therapy, EGFR targeting, cancer metabolism, enzyme engineering, targeted therapy

Introduction

Cancer progression is driven by extensive metabolic reprogramming that supports sustained proliferation, adaptation to environmental stress, and resistance to therapeutic intervention [1, 2]. One prominent consequence of such reprogramming is an increased reliance on specific amino acids, which creates exploitable metabolic vulnerabilities in malignant cells [3]. Deprivation of amino acids, including L-methionine (L-Met), asparagine, arginine, and lysine, disrupts essential cellular processes such as protein synthesis, redox homeostasis, nucleotide biosynthesis, and epigenetic regulation [4–7]. The clinical success of L-asparaginase in acute lymphoblastic leukemia provides rationale for amino acid depletion as an

effective therapeutic strategy and stimulated the exploration of similar approaches targeting additional metabolic dependencies across diverse cancer types [8–11].

L-Met addiction, known as the Hoffman effect [12], represents a well-characterized metabolic phenotype in which cancer cells exhibit a strict dependence on exogenous L-Met for proliferation despite retaining the capacity to regenerate L-Met from homocysteine [13, 14]. This apparent paradox arises from an increased demand for methyl group donors required to sustain elevated transmethylation reactions, which support aberrant DNA and histone methylation, RNA modification, and polyamine biosynthesis [13, 14]. As a consequence, restriction of L-Met availability has emerged as a promising anticancer strategy. Among the available approaches, enzymatic depletion using recombinant methionine γ-lyase (rMGL; EC 4.4.1.11) has received considerable attention [3, 15, 16]. rMGL catalyzes the γ-elimination of L-Met to generate α-ketobutyrate, ammonia, and methanethiol, thereby reducing systemic L-Met levels and suppressing tumor growth in multiple preclinical models [17–21].

Despite encouraging preclinical outcomes, clinical translation of rMGL-based therapies remains limited by several challenges. The bacterial origin of the enzyme contributes to immunogenic responses that restrict repeated administration. In addition, rapid proteolytic degradation and short circulating half-life reduce systemic exposure and therapeutic efficacy. Non-selective depletion of L-Met may also affect normal proliferating tissues, raising safety concerns, while insufficient tumor accumulation limits therapeutic selectivity [22]. Various strategies have been explored to overcome these limitations, including PEGylation, encapsulation within erythrocytes, oral delivery approaches, and protein engineering through peptide fusion [15].

Targeted protein engineering has emerged as a promising strategy to enhance the therapeutic performance of enzymatic anticancer agents [23]. Fusion of short targeting peptides can facilitate receptor-mediated localization to tumor cells, thereby increasing local enzymatic activity while minimizing systemic exposure. The epidermal growth factor receptor (EGFR) represents a relevant target in this context due to its frequent overexpression and accessibility on the surface of a wide range of solid tumors [24].

In our previous work, an engineered variant of rMGL, designated rMGL-S3 (engineered rMGL fused with S3 peptide), was developed by fusing a 16-amino-acid peptide (RCSHGYTGIRCQAVVL) derived from the VGF protein to the C-terminus of the wild-type enzyme. The design aimed to enhance interaction with EGFR and improve tumor-associated localization, thereby addressing limitations related to targeting and efficacy [25, 26]. The present study evaluates the antitumor activity of rMGL-S3 using in vitro and in vivo models, with the objective of assessing its potential as a targeted L-Met-depleting therapeutic strategy.

Materials and methods

Biosynthesis and enzyme assays for rMGL and rMGL-S3

Expression and purification of rMGL from *Clostridium sporogenes* and its engineered variant rMGL-S3 were performed in *Escherichia coli* BL21-Gold(DE3) cells (Agilent) transformed with pET-mgl-Sporog or pET-mgl-S3 plasmids, respectively. The rMGL-S3 construct was generated by fusing a 16-amino-acid peptide (RCSHGYTGIRCQAVVL) [27], derived from the VGF protein, to the C-terminus of the wild-type enzyme. Synthesis and purification of the enzymes were performed according to Bondarev et al. [26]. Enzymatic activity was determined using a coupled spectrophotometric assay based on the γ-elimination reaction of L-Met. The reaction was monitored by measuring the decrease in NADH absorbance at 340 nm (ε = 6,220 M^{-1} cm^{-1}) at 30°C [28]. The assay mixture contained 100 mM potassium phosphate buffer (pH 8.0), 0.2 mM NADH, 20 mM L-Met, and a coupling dehydrogenase to enable indirect quantification of α-ketobutyrate formation [29]. One unit of enzyme activity was defined as the amount of enzyme catalyzing the formation of 1 μmol of α-ketobutyrate per minute under the specified conditions. Specific activity of the purified enzymes was determined to be 9.3 U/mg for wild-type rMGL and 7.0 U/mg for rMGL-S3, indicating a moderate reduction in catalytic efficiency following C-terminal modification. All measurements were performed in triplicate, and results are reported as mean values.

Cell lines and cytotoxicity evaluation

The cytotoxic activity of rMGL and its engineered variant rMGL-S3 was evaluated across a panel of human cancer cell lines, including HCT116 (colon adenocarcinoma), DU145 and PC3 (prostate carcinoma), MCF7 and MDA-MB-231 (breast carcinoma), as well as Panc1 and MIA PaCa-2 (pancreatic carcinoma), all obtained from the ATCC, which performs rigorous STR authentication per batch to confirm the absence of cross-contamination. All lines were routinely tested for mycoplasma using the MycoAlert™ PLUS kit (Lonza) and consistently found negative. Cells were cultured in RPMI-1640 medium (PanEco, Russia) supplemented with 10% fetal bovine serum (HyClone, UK), 2 mM L-glutamine, and 100 U/mL penicillin (PanEco, Russia), and maintained at 37°C in a humidified atmosphere containing 5% CO_2.

Cells in the exponential growth phase were harvested using trypsinization and seeded into 96-well plates at a density of 4–6 × 10^3 cells per well. After 24 h of incubation, rMGL or rMGL-S3 was added in two-fold serial dilutions ranging from 4 to 128 mU/mL. Enzyme solutions were prepared in sterile phosphate-buffered saline (PBS; pH 7.4) supplemented with 0.5 mM pyridoxal-5'-phosphate (PLP). Following enzyme addition, cells were incubated for 60 min at 37°C. Unbound enzymes were removed by washing three times with RPMI-1640 medium containing 0.5 mM PLP. Cells were then cultured for an additional 72 h under standard conditions.

Cell viability was assessed using the MTT assay. Absorbance was measured at 540 nm using a Multiskan™ FC microplate reader (Thermo Scientific, Waltham, MA, USA). Untreated cells receiving PBS served as a negative control, while continuous exposure to the enzyme without washing was used as a positive control. All experiments were performed in triplicate (n = 3), and results were expressed as mean values.

Cell cycle analysis

Cell cycle analysis of A431 and triple-negative breast cancer cell line MDA-MB-468 was assessed using a standard propidium iodide (PI) staining protocol, as previously described [30]. Briefly, 5 × 10^5 cells were seeded into each well of a 6-well plate and allowed to adhere for 24 h. Subsequently, cells were treated with the indicated proteins in triplicate and incubated for an additional 48 h. Following treatment, cells were harvested by trypsinization, washed, and fixed in 70% ethanol to achieve permeabilization. Fixed cells were then stained with PI (50 μg/mL) in the presence of RNase A (10 μg/mL) to eliminate RNA interference. Finally, DNA content was analyzed by flow cytometry using an Attune NxT system (Thermo Fisher Scientific, USA). All experiments were performed in triplicate (n = 3).

Animals and evaluation of antitumor activity

Female BALB/c nude mice (6–8 weeks old, 20 ± 2 g) were obtained and housed in the animal facility of N.N. Blokhin National Medical Research Center of Oncology under specific pathogen-free conditions with controlled temperature and humidity and provided with a standard diet and water ad libitum. All experimental procedures were conducted in compliance with EU Directive 2010/63/EU and approved by the Institutional Animal Care and Use Committee of the N.N. Blokhin National Medical Research Center of Oncology (Protocol No. 2025-5a of 16.12.2025). For terminal procedures, mice were deeply anesthetized with 5% isoflurane via inhalation, followed by cervical dislocation. Death was confirmed by cervical separation and the absence of respiration and heartbeat.

Human cancer cells, including A431, HCT116, and Panc1, were suspended at a density of 5–6 × 10^6 cells in 0.2 mL of RPMI-1640 medium devoid of fetal bovine serum and subsequently transplanted s.c. into the flank region using a trocar needle. Tumor growth was monitored, and treatment was initiated once tumor volume reached approximately 100 mm^3 at 12-, 8-, and 6-day post-inoculation for A431, HCT116, and Panc1, respectively. Animals were randomly assigned to six experimental groups (n = 5 per group for each tumor model). rMGL and rMGL-S3 were prepared in sterile PBS (pH 7.4) supplemented with 0.5 mM PLP: Group 1 received intraperitoneal (IP) administration of PBS once daily for three weeks and served as vehicle control; Group 2 received rMGL-S3 at a dose of 2,000 U/kg via IP injection once daily for three

weeks; Group 3 received rMGL-S3 at 1,000 U/kg via IP injection following the same schedule; Group 4 received rMGL at 2,000 U/kg via IP injection once daily for three weeks; Group 5 received rMGL-S3 at 1,000 U/kg via intravenous (IV) administration every 48 hours for three weeks; and Group 6 received rMGL at 1,000 U/kg via IV administration at the same interval. The doses of rMGL and rMGL-S3 were selected based on our preliminary dose-finding studies (data not shown). The 2,000 U/kg dose was the maximum tolerable dose without adverse effects, while the 1,000 U/kg dose was chosen to assess dose-dependent efficacy and permit comparison with earlier studies using unmodified rMGL.

Tumor volume and body weight measurements

Tumor dimensions were recorded twice weekly throughout the treatment period using caliper measurements. Tumor volume was estimated according to the ellipsoid equation, (length × width × height × π)/6, and mean tumor volumes for each experimental group were used to generate growth curves. Therapeutic efficacy was quantified as tumor growth inhibition (TGI), calculated as TGI (%) = [(Vc − Ve)/Vc] × 100, where Vc and Ve denote the mean tumor volumes of the control and treated groups, respectively. Treatment tolerability was monitored throughout the study by serial body weight measurements and daily appearance monitoring.

Statistical analysis

Statistical analyses for the in vitro experiments were carried out in triplicate. GraphPad Prism version 9.0 was used to determine the IC_{50}. The data of IC_{50} are presented as mean ± standard deviation (M ± SD).

Statistical analysis of in vivo data was conducted using IBM SPSS Statistics. Differences between control and treatment groups were evaluated using the non-parametric Mann–Whitney *U* test. Data are presented as M ± SD, and graphical representations include line and bar plots with corresponding error bars. The probability value (p) was computed to compare the control group with each treatment group; $p < 0.05$ was considered statistically significant.

Results

Cytotoxic activity of rMGL-S3 and rMGL across various human cancer cell lines

The antiproliferative activity of rMGL and its engineered variant rMGL-S3 was evaluated using a panel of human cancer cell lines representing HCT116, MCF7, MDA-MB-231, DU145, PC3, Panc1, and MIA PaCa-2. Cytotoxicity was assessed under two experimental conditions, including continuous exposure and a washing protocol designed to remove unbound enzyme following initial incubation (See Cell lines and cytotoxicity evaluation).

Under continuous exposure conditions, both rMGL and rMGL-S3 exhibited comparable cytotoxic effects across all tested cell lines, with IC_{50} values ranging from 8.4 to 47.8 mU/mL (Table 1). The highest sensitivity was observed in Panc1 cells, whereas breast cancer cell lines demonstrated lower responsiveness.

Table 1. Cytotoxicity of rMGL-S3 and rMGL across various human cancer cell lines.

Organ	Cell line	IC_{50} (mU/mL)			
		Without washing		After washing	
		rMGL-S3	rMGL	rMGL-S3	rMGL
Colon adenocarcinoma	HCT116	27.2 ± 2.4	29.4 ± 1.9	32.7 ± 0.7	> 128
Breast cancer	MCF7	38.7 ± 1.7	34.8 ± 3.1	> 128	> 128
	MDA-MB-231	41.3 ± 2.4	47.8 ± 2.4	68.4 ± 2.7	> 128
Prostate cancer	DU145	16.8 ± 1.3	20.1 ± 2.9	19.3 ± 0.9	> 128
	PC3	28.1 ± 2.2	30.8 ± 2.4	44.7 ± 0.7	> 128
Pancreatic cancer	Panc1	8.4 ± 1.7	13.8 ± 1.1	10.3 ± 1.1	> 128
	MIA PaCa-2	24.3 ± 0.4	27.9 ± 1.8	48.8 ± 2.0	> 128

In contrast, marked differences between the two enzymes were observed following removal of unbound protein (See Cell lines and cytotoxicity evaluation). rMGL-S3 retained significant cytotoxic activity across multiple cell lines, whereas rMGL exhibited no detectable activity (IC_{50} > 128 mU/mL) under identical washing conditions (Table 1). Among pancreatic cancer models, Panc1 cells showed the greatest sensitivity to rMGL-S3 (IC_{50} = 10.3 ± 1.1 mU/mL), while MIA PaCa-2 cells were less responsive (IC_{50} = 48.8 ± 2.0 mU/mL). A similar pattern was observed in prostate cancer models, where DU145 cells demonstrated higher sensitivity (IC_{50} = 19.3 ± 0.9 mU/mL) compared to PC3 cells (IC_{50} = 44.7 ± 0.7 mU/mL).

Breast cancer cell lines exhibited reduced sensitivity following washing, with MDA-MB-231 showing moderate sensitivity (IC_{50} = 68.4 ± 2.7 mU/mL), while MCF7 cells displayed no measurable response within the tested concentration range. In colorectal cancer, HCT116 cells remained responsive to rMGL-S3 (IC_{50} = 32.7 ± 0.7 mU/mL), whereas rMGL failed to demonstrate detectable activity. Notably, high cytotoxic activity of rMGL-S3 was also observed in A431 epidermoid carcinoma cells (IC_{50} = 9.35 mU/mL) [26], further supporting enhanced functional retention following washing.

Following removal of unbound enzyme, rMGL-S3 retained substantial cytotoxic activity, whereas no measurable activity was detected for the parental rMGL under identical experimental conditions. Together with our previously reported in vitro evidence of S3-mediated receptor binding [26], the present findings support receptor-directed localization as a mechanism that prolongs enzyme residence at the tumor cell surface and sustains antiproliferative activity.

Cell cycle measurement of rMGL-S3 and rMGL against A431 and MDA-MB-468 cell lines

To evaluate the impact of rMGL or rMGL-S3 on cell cycle progression, two EGFR-overexpressing cancer cell lines, A431 and MDA-MB-468, were analyzed (Figure 1).

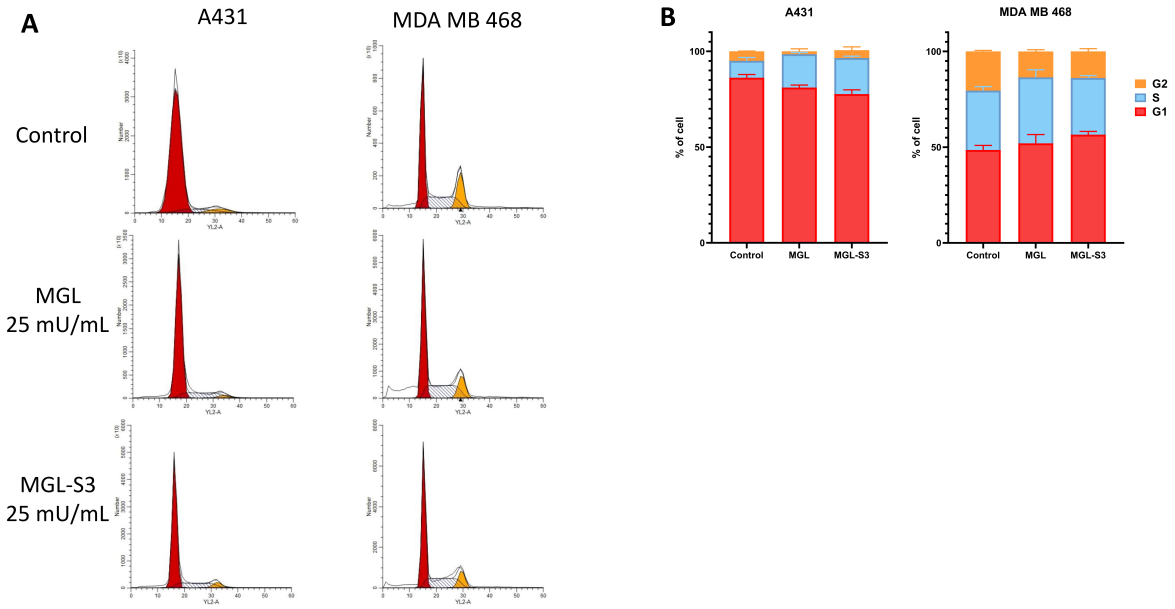

Figure 1. Cell cycle analysis of A431 and MDA-MB-468 cells treated with rMGL-S3 and rMGL. (**A**) Representative flow cytometry histograms of propidium iodide fluorescence illustrating DNA content distribution and cell cycle profiles in A431 and MDA-MB-468 cells following treatment; (**B**) Quantitative analysis of cell cycle phase distribution (G_1, S, and G_2/M phases). Data are presented as mean ± SD of triplicate experiments, with statistical significance indicated relative to the control group.

In A431 cells, treatment with rMGL and rMGL-S3 resulted in a statistically significant slight reduction in the G_1 phase compared to the control group (86.23% vs. 81.09% for rMGL and 77.70% for rMGL-S3; p = 0.0138 and p = 0.0058, respectively). Consistently, a marked increase in the S phase fraction was observed

following treatment (8.81% in control vs. 17.44% for rMGL and 18.78% for rMGL-S3; $p = 0.0015$ and p = 0.0010, respectively), suggesting enhanced entry into DNA synthesis. In the G_2 phase, rMGL treatment led to a significant decrease (4.96% in control vs. 1.47%; $p = 0.01$), whereas rMGL-S3 had no significant effect (4.15%; $p = 0.4653$). The relatively low baseline proportion of G_2-phase cells in the control group likely reflects high cell density and contact inhibition at confluence.

In contrast, MDA-MB-468 cells exhibited a distinct response profile. rMGL-S3 treatment induced significant G_1 phase accumulation (48.53% in control vs. 56.55%, $p = 0.0086$), while rMGL showed a similar though non-significant trend (51.99%, $p = 0.3125$). Concurrently, both rMGL and rMGL-S3 significantly reduced the proportion of cells in the G_2/M phase (20.28% in control vs. 13.56% for rMGL and 13.86% for rMGL-S3; $p = 0.0003$ and $p = 0.0018$, respectively). No statistically significant differences were observed in the S phase between treated and control groups (30.98% in control vs. 34.43% for rMGL and 29.58% for rMGL-S3; $p = 0.3116$ and $p = 0.1759$, respectively).

Collectively, these findings indicate that the treatments exert cell line—dependent effects on cell cycle progression, promoting S phase accumulation in A431 cells while inducing G_1 phase accumulation in MDA-MB-468 cells.

In vivo antitumor activity in A431 xenograft model

Antitumor efficacy of rMGL and rMGL-S3 was evaluated in the A431 xenograft model. Tumor growth demonstrated a pronounced suppression of xenograft growth in animals treated with rMGL-S3 compared with control and rMGL groups (Figure 2).

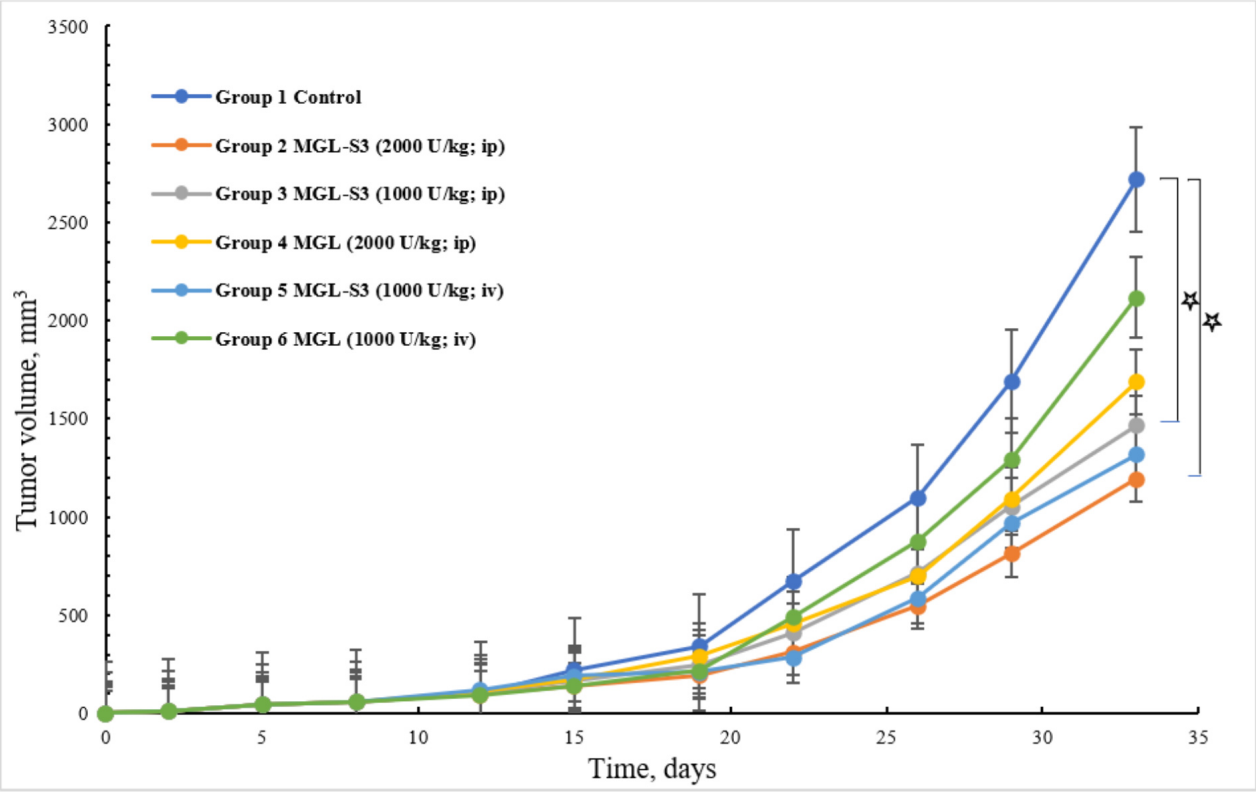

Figure 2. Effects of rMGL-S3 and rMGL on BALB/c nude mice ($n = 5$ per group) bearing A431 xenografts. (The asterisk symbol represents $p < 0.05$). ip: intraperitoneal; iv: intravenous.

IP administration of rMGL-S3 at 2,000 U/kg significantly reduced tumor volume (1,196.3 ± 82.8 mm^3) compared with vehicle-treated controls (2,719.6 ± 144.5 mm^3), achieving 56% TGI ($p = 0.032$). A lower IP dose of rMGL-S3 (1,000 U/kg) also produced a statistically significant antitumor effect, with a mean tumor volume of 1,467.6 ± 93.6 mm^3 and a TGI of 46% ($p = 0.028$). IV administration of rMGL-S3 at 1,000 U/kg led to a comparable reduction in tumor growth (1,320.1 ± 391 mm^3; TGI 51%); however, statistical significance was not achieved.

In contrast, treatment with rMGL demonstrated limited antitumor activity. IP administration at 2,000 U/kg resulted in moderate TGI (38%) without statistical significance, while IV administration at 1,000 U/kg showed minimal efficacy, with tumor volumes (2,118.9 ± 288 mm^3) approaching control levels (TGI 22%; $p > 0.05$).

Comparative analysis across treatment groups indicates superior efficacy of rMGL-S3 over rMGL, particularly following IP administration at higher doses. Enhanced antitumor activity may reflect improved tumor localization and retention associated with the engineered construct. Evaluation of treatment tolerability demonstrated stable body weight across all groups throughout the study period, with no observable signs of systemic toxicity. Maintenance of physiological body mass supports a favorable safety profile under the applied dosing regimens.

In vivo antitumor activity in HCT116 xenograft model

Antitumor efficacy of rMGL and rMGL-S3 was further evaluated in the HCT116 xenograft model. Tumor growth analysis demonstrated a dose- and route-dependent response, with rMGL-S3 consistently outperforming rMGL (Figure 3).

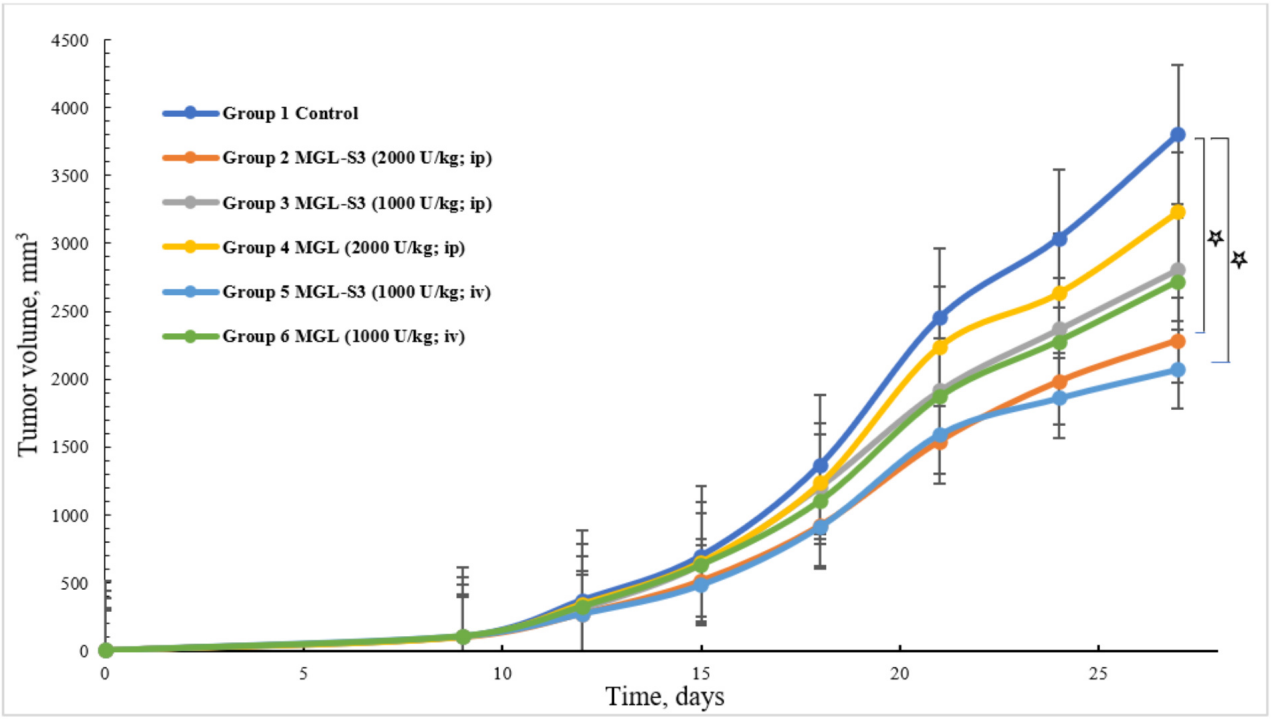

Figure 3. Effects of rMGL-S3 and rMGL on BALB/c nude mice (n = 5 per group) bearing HCT116 xenografts. (The asterisk symbol represents $p < 0.05$). ip: intraperitoneal; iv: intravenous.

IP administration of rMGL-S3 at 2,000 U/kg resulted in a significant reduction in tumor volume (2,285.5 ± 220.3 mm^3) compared with the vehicle group (3,799.5 ± 302.1 mm^3), corresponding to TGI of 40% ($p < 0.05$). A lower IP dose of rMGL-S3 (1,000 U/kg) produced a moderate decrease in tumor burden (2,808.1 ± 151.3 mm^3; TGI 26.1%); however, statistical significance was not achieved ($p = 0.343$), indicating a reduced therapeutic effect at lower dosing via this route.

In contrast, IV administration of rMGL-S3 at 1,000 U/kg demonstrated enhanced antitumor activity, with a significant reduction in tumor volume (2,072.6 ± 142.5 mm^3) with TGI of 45% ($p = 0.029$). The improved efficacy observed with IV delivery suggests a potential advantage in systemic distribution and tumor accessibility for the engineered enzyme.

rMGL exhibited limited therapeutic activity across both administration routes. IP delivery at 2,000 U/kg resulted in minimal TGI (15%) without statistical significance, while IV administration at 1,000 U/kg

produced a modest effect (2,718.4 ± 169.4 mm^3; TGI 28%; $p > 0.114$). Body weight remained stable throughout the treatment period, with no visible signs of systemic toxicity. Overall, rMGL-S3 demonstrated superior antitumor efficacy compared with the rMGL, particularly when administered IV.

In vivo antitumor activity in Panc1 xenograft model

Antitumor efficacy of rMGL and the engineered variant (rMGL-S3) was evaluated in the Panc1 xenograft model. Tumor growth analysis revealed a moderate but consistent inhibitory effect associated with rMGL-S3 treatment, with variation depending on dose and route of administration (Figure 4).

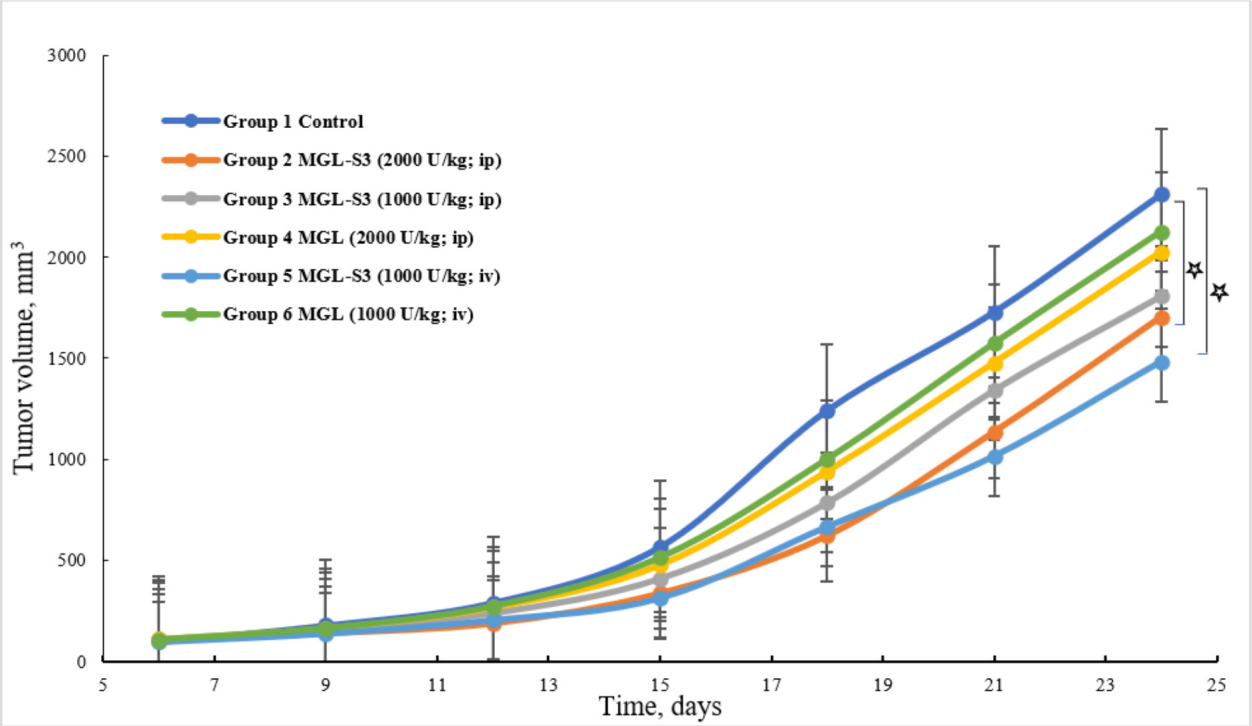

Figure 4. Effects of rMGL-S3 and rMGL on BALB/c nude mice (n = 5 per group) bearing Panc1 xenografts. (The asterisk symbol represents $p < 0.05$). ip: intraperitoneal; iv: intravenous.

IP administration of rMGL-S3 at 2,000 U/kg resulted in a significant reduction in tumor volume (1,701.0 ± 620.8 mm^3) compared with the vehicle group (2,309.4 ± 745.5 mm^3), corresponding to TGI of 26% ($p < 0.05$). A lower IP dose (1,000 U/kg) produced a comparable reduction in tumor burden (1,805.7 ± 575.3 mm^3; TGI 21.8%); however, statistical significance was not achieved ($p = 0.234$), indicating a dose-dependent response with reduced efficacy at lower exposure levels.

IV administration of rMGL-S3 at 1,000 U/kg demonstrated improved antitumor activity relative to IP delivery, resulting in a tumor volume of 1,480.8 ± 429.5 mm^3 and a TGI of 36% ($p = 0.05$). Enhanced efficacy associated with IV administration suggests improved systemic distribution and tumor accessibility of the engineered enzyme in the pancreatic tumor model.

rMGL exhibited limited therapeutic activity. IP administration at 2,000 U/kg resulted in minimal TGI (12%) without statistical significance, while IV administration at 1,000 U/kg produced a marginal effect (2,124.6 ± 686.7 mm^3; TGI 8%; $p > 0.114$). Comparative analysis indicates superior performance of rMGL-S3 over the rMGL across all treatment conditions.

Discussion

The present study provides comprehensive preclinical validation of the previously engineered EGFR-targeting rMGL-S3 across complementary in vitro and in vivo cancer models. Our key findings include: (i) rMGL-S3 maintains cytotoxic activity following removal of unbound enzyme across multiple cancer cell

lines, whereas unmodified rMGL completely loses activity under identical conditions; (ii) rMGL-S3 induces cell line-dependent cell cycle perturbations, promoting S phase accumulation in A431 cells while inducing G_1 phase accumulation in MDA-MB-468 cells; (iii) in vivo, rMGL-S3 achieves superior TGI compared with unmodified rMGL in A431, HCT116, and Panc1 xenograft models; and (iv) the enhanced efficacy correlates with EGFR expression levels, supporting a receptor-mediated mechanism.

Amino acid deprivation therapy (AADT) based on exogenous enzymes has emerged as a promising therapeutic strategy because malignant cells exhibit metabolic dependencies that distinguish them from normal tissues [3]. Despite encouraging preclinical outcomes, clinical translation remains limited by insufficient tumor-selective delivery, which reduces therapeutic efficacy and increases systemic toxicity [31]. Peptide-mediated targeting has therefore attracted considerable interest as an approach to enhance tumor localization through interactions with overexpressed cell-surface receptors, including EGFR and integrins.

Peptide-mediated targeting represents a well-established approach to enhance tumor localization of therapeutic agents through interaction with overexpressed surface receptors, including EGFR and integrins [32, 33]. In our previous studies, an engineered variant of rMGL, referred to as rMGL-S3, was developed through fusion with a VGF-derived peptide designed to promote receptor interaction and stable association with the cancer cell surface [25, 26]. Such design aimed to couple metabolic disruption with receptor-mediated targeting, thereby improving selectivity and functional retention. Importantly, prior evaluation of rMGL-S3 in non-malignant HEK293 cells demonstrated the same cytotoxicity of rMGL, supporting its selectivity toward cancer cells [26]. This selectivity is consistent with observations in other amino acid depletion strategies and may be further enhanced by the receptor-mediated targeting mechanism. The potential role of nanoparticle-like interactions [34] or conditioned media modulation in cell association remains to be investigated and could provide additional insights into the mechanism of selective tumor association.

Findings from the present study provide further mechanistic insight into the functional properties of rMGL-S3. Sustained cytotoxic activity following removal of unbound enzyme was observed in cancer cell lines characterized by overexpression of EGFR, including A431, Panc1, and DU145 [35], indicating stable surface association and prolonged functional activity. In contrast, unmodified rMGL did not exhibit measurable cytotoxic effects under equivalent conditions, confirming that the fusion peptide is essential for effective cell surface retention. Reduced sensitivity in MCF7 and PC3 cells, which are associated with comparatively lower receptor expression [35], further supports a dependence on receptor availability. Such observations align with a model in which the VGF-derived S3 peptide mediates receptor-dependent anchoring of the octameric enzyme complex, enabling localized L-Met depletion at the tumor interface and sustaining antiproliferative effects beyond systemic clearance.

A moderate reduction in the specific activity of rMGL-S3 relative to the parental enzyme did not compromise therapeutic efficacy. Instead, enhanced antitumor activity suggests that effective biological performance is governed not only by intrinsic catalytic efficiency but also by pharmacological factors that determine enzyme availability at the tumor site. The sustained cytotoxic activity observed following removal of unbound enzyme supports the concept that prolonged tumor-associated retention can compensate for reduced specific activity by extending the duration of local methionine depletion.

The distinct cell cycle responses elicited by rMGL and rMGL-S3 underscore the context-dependent nature of L-Met depletion in regulating proliferative dynamics. Rather than inducing a uniform cell cycle blockade, L-Met restriction appears to interfere with different regulatory checkpoints depending on the cellular background. This variability likely reflects differences in metabolic dependencies, cell cycle control mechanisms, and the integration of nutrient-sensing pathways across tumor types. In A431 cells, the observed pattern is consistent with impaired progression through DNA synthesis, suggesting that L-Met availability may be particularly critical for sustaining replication-associated processes in A431 cells. Depletion of L-Met could disrupt nucleotide biosynthesis or replication stress responses, thereby constraining efficient cell cycle progression. In contrast, the response in MDA-MB-468 cells points toward a

restriction at the level of cell cycle entry, implying that L-Met depletion may more strongly influence early checkpoint regulation in MDA-MB-468 cells. Taken together, these findings highlight that the antiproliferative effects of L-Met-degrading enzymes are not solely cytotoxic but involve modulation of cell cycle control in a cell type-specific manner.

In vivo data provide additional support for this proposed mechanism. Substantial TGI was observed in xenograft models characterized by high receptor expression, as demonstrated in the A431 model [35], where IP administration of rMGL-S3 at 2,000 U/kg resulted in significant suppression of tumor progression, whereas unmodified rMGL exhibited limited efficacy. This observation is consistent with our prior in vitro findings in the same model, in which rMGL-S3 exhibited pronounced cytotoxic activity with a low IC_{50} value of 9.35 mU/mL [26], reinforcing the relationship between receptor expression, enzyme targeting, and therapeutic response across experimental systems. Comparable results were obtained in the Panc1 model, where rMGL-S3 induced measurable TGI following IV administration, whereas the unmodified enzyme exerted minimal effect. In contrast, reduced efficacy in the HCT116 model, which is associated with comparatively lower receptor expression [35], further indicates that the magnitude of therapeutic response is closely linked to receptor availability.

The observed correlation between EGFR expression levels and the therapeutic activity of rMGL-S3 supports, but does not definitively establish, a receptor-mediated mechanism. Together with our previous in vitro characterization of S3-mediated EGFR binding, the present findings are consistent with the hypothesis that receptor-directed localization enhances the functional persistence of rMGL-S3 at the tumor site. Direct in vivo validation of receptor engagement through receptor-blocking experiments or molecular imaging approaches will be required to confirm the proposed targeting mechanism and further define its contribution to the enhanced therapeutic efficacy observed in the present study.

Structural organization of rMGL-S3 [25, 26] contributes to its functional properties. Formation of an octameric assembly, as previously reported [25], enables multivalent interactions with cell surface receptors, thereby increasing binding avidity and promoting sustained retention at the tumor interface. Such multivalency is particularly advantageous in the context of heterogeneous receptor expression and may underlie the prolonged biological activity observed for the engineered enzyme [15, 36, 37].

Localization of enzymatic activity at the tumor surface represents a key advantage over approaches that primarily aim to extend systemic circulation. Accumulation of rMGL-S3 within tumor regions may facilitate the formation of localized L-Met depletion gradients, particularly in poorly vascularized areas, thereby enhancing antitumor efficacy while limiting systemic exposure. Such spatially restricted activity provides a plausible mechanistic basis for the improved therapeutic performance observed.

The favorable tolerability observed in the present study, reflected by stable body weight and the absence of overt clinical signs of toxicity, is consistent with previous reports describing acceptable safety profiles of methionine γ-lyase-based therapies in murine models [15]. Recent studies have also highlighted the capacity of enzyme-based therapeutic strategies to modulate inflammatory responses in preclinical disease models [38, 39]. Although inflammatory biomarkers were not evaluated in the present study, future investigations should determine whether similar immunological effects contribute to the therapeutic profile of rMGL-S3.

While our study demonstrates the antiproliferative and cell cycle-modulating effects of rMGL-S3, future investigations should explore the effects on tumor cell migration, invasion, and downstream signaling pathways, particularly EGFR-mediated signal transduction and its modulation by methionine depletion. Such studies would further elucidate the molecular basis of the enhanced therapeutic activity observed and could identify combination strategies with targeted agents affecting these pathways.

The present study provides comprehensive preclinical validation of the engineered rMGL-S3 across complementary in vitro and in vivo cancer models. Receptor-directed localization enhanced the antitumor activity of methionine γ-lyase while maintaining favorable tolerability, supporting the therapeutic potential of targeted methionine depletion. Although further optimization of pharmacokinetic properties,

immunogenicity, and clinical applicability remains necessary, the present findings establish a strong preclinical foundation for the continued development of receptor-targeted enzymatic AADT.

Abbreviations

AADT: amino acid deprivation therapy

EGFR: epidermal growth factor receptor

IP: intraperitoneal

IV: intravenous

L-Met: L-methionine

PBS: phosphate-buffered saline

PI: propidium iodide

PLP: pyridoxal-5'-phosphate

rMGL: recombinant methionine γ-lyase

rMGL-S3: engineered rMGL fused with S3 peptide

TGI: tumor growth inhibition

Declarations

Acknowledgments

NAB, MMB and IVM acknowledge the support from the Ministry of Science and Higher Education of the Russian Federation (agreement 075-03-2026-305, project FSMG-2025-0003).

Author contributions

LAQ: Writing—original draft, Investigation. AY: Investigation. NAB: Investigation. MMB: Investigation. IVM: Conceptualization, Writing—review & editing. VSP: Supervision, Writing—review & editing. All authors read and approved the submitted version.

Conflicts of interest

The authors declare no conflict of interest, financial or otherwise.

Ethical approval

All animal experimental procedures were approved by the Institutional Animal Care and Use Committee of the N.N. Blokhin National Medical Research Center of Oncology (Protocol No. 2025-5a of 16.12.2025).

Consent to participate

Not applicable.

Consent to publication

Not applicable.

Availability of data and materials

The datasets supporting the findings of this study are available from the corresponding author upon reasonable request.

Funding

This study received financial support from the Ministry of Health State Research Program [NYUO-2026-0043]. The funders had no role in study design, data collection and analysis, decision to publish, or preparation of the manuscript.

Copyright

© The Author(s) 2026.

Publisher's note

Open Exploration maintains a neutral stance on jurisdictional claims in published institutional affiliations and maps. All opinions expressed in this article are the personal views of the author(s) and do not represent the stance of the editorial team or the publisher.

References

1. Macintyre AN, Rathmell JC. Activated lymphocytes as a metabolic model for carcinogenesis. Cancer Metab. 2013;1:5. [DOI] [PubMed] [PMC]
2. Schiliro C, Firestein BL. Mechanisms of Metabolic Reprogramming in Cancer Cells Supporting Enhanced Growth and Proliferation. Cells. 2021;10:1056. [DOI] [PubMed] [PMC]
3. Morozova EA, Kulikova VV, Yashin DV, Anufrieva NV, Anisimova NY, Revtovich SV, et al. Kinetic Parameters and Cytotoxic Activity of Recombinant Methionine γ-Lyase from Clostridium tetani, Clostridium sporogenes, Porphyromonas gingivalis and Citrobacter freundii. Acta Naturae. 2013;5: 92–8. [PubMed] [PMC]
4. Latimer MN, Freij KW, Cleveland BM, Biga PR. Physiological and Molecular Mechanisms of Methionine Restriction. Front Endocrinol. 2018;9:217. [DOI] [PubMed] [PMC]
5. Li X, Zhang HS. Amino acid metabolism, redox balance and epigenetic regulation in cancer. FEBS J. 2023;291:412–29. [DOI] [PubMed]
6. Krall AS, Xu S, Graeber TG, Braas D, Christofk HR. Asparagine promotes cancer cell proliferation through use as an amino acid exchange factor. Nat Commun. 2016;7:11457. [DOI] [PubMed] [PMC]
7. Feng T, Xie F, Lyu Y, Yu P, Chen B, Yu J, et al. The arginine metabolism and its deprivation in cancer therapy. Cancer Lett. 2025;620:217680. [DOI] [PubMed]
8. Gay F, Aguera K, Sénéchal K, Tainturier A, Berlier W, Maucort-Boulch D, et al. Methionine tumor starvation by erythrocyte-encapsulated methionine gamma-lyase activity controlled with per os vitamin B6. Cancer Med. 2017;6:1437–52. [DOI] [PubMed] [PMC]
9. Yoon JK, Frankel AE, Feun LG, Ekmekcioglu S, Kim KB. Arginine deprivation therapy for malignant melanoma. Clin Pharmacol: Adv Appl. 2012;5:11–9. [DOI] [PubMed] [PMC]
10. Synakiewicz A, Stachowicz-Stencel T, Adamkiewicz-Drozynska E. The role of arginine and the modified arginine deiminase enzyme ADI-PEG 20 in cancer therapy with special emphasis on Phase I/ II clinical trials. Expert Opin Investig Drugs. 2014;23:1517–29. [DOI] [PubMed]
11. Whitecar JP Jr, Bodey GP, Harris JE, Freireich EJ. L-Asparaginase. N Engl J Med. 1970;282:732–4. [DOI] [PubMed]
12. Kaiser P. Methionine Dependence of Cancer. Biomolecules. 2020;10:568. [DOI] [PubMed] [PMC]
13. Hoffman RM, Erbe RW. High in vivo rates of methionine biosynthesis in transformed human and malignant rat cells auxotrophic for methionine. Proc Natl Acad Sci. 1976;73:1523–7. [DOI] [PubMed] [PMC]
14. Hoffman RM. Development of recombinant methioninase to target the general cancer-specific metabolic defect of methionine dependence: a 40-year odyssey. Expert Opin Biol Ther. 2014;15: 21–31. [DOI] [PubMed]
15. Abo Qoura L, Balakin KV, Hoffman RM, Pokrovsky VS. The potential of methioninase for cancer treatment. Biochim Biophys Acta (BBA) - Rev Cancer. 2024;1879:189122. [DOI] [PubMed]
16. Pokrovsky VS, Abo qoura L, Demidova EA, Han Q, Hoffman RM. Methionine addiction of cancer cells targeted by methioninase. Biochemisty (Mosc.). 2023;88:1162–72. [DOI]

17. Han Q, Hoffman RM. Chronic Treatment of an Advanced Prostate-cancer Patient With Oral Methioninase Resulted in Long-term Stabilization of Rapidly Rising PSA Levels. In Vivo. 2021;35: 2171–6. [DOI] [PubMed] [PMC]
18. Kubota Y, Han Q, Hamada K, Aoki Y, Masaki N, Obara K, et al. Long-term Stable Disease in a Rectal-cancer Patient Treated by Methionine Restriction With Oral Recombinant Methioninase and a Low-methionine Diet. Anticancer Res. 2022;42:3857–61. [DOI] [PubMed]
19. Kubota Y, Han Q, Hozumi C, Masaki N, Yamamoto J, Aoki Y, et al. Stage IV Pancreatic Cancer Patient Treated With FOLFIRINOX Combined With Oral Methioninase: A Highly-Rare Case With Long-term Stable Disease. Anticancer Res. 2022;42:2567–72. [DOI] [PubMed]
20. Kubota Y, Han Q, Masaki N, Hozumi C, Hamada K, Aoki Y, et al. Elimination of Axillary-Lymph-Node Metastases in a Patient With Invasive Lobular Breast Cancer Treated by First-line Neo-adjuvant Chemotherapy Combined With Methionine Restriction. Anticancer Res. 2022;42:5819–23. [DOI] [PubMed]
21. Tan Y, Xu M, Tan X, Tan X, Wang X, Saikawa Y, et al. Overexpression and Large-Scale Production of Recombinantl-Methionine-α-deamino-γ-mercaptomethane-lyase for Novel Anticancer Therapy. Protein Expr Purif. 1997;9:233–45. [DOI] [PubMed]
22. Yang Z, Wang J, Lu Q, Xu J, Kobayashi Y, Takakura T, et al. PEGylation Confers Greatly Extended Half-Life and Attenuated Immunogenicity to Recombinant Methioninase in Primates. Cancer Res. 2004;64: 6673–8. [DOI] [PubMed]
23. Naderiyan Z, Shoari A. Protein Engineering Paving the Way for Next-Generation Therapies in Cancer. Int J Transl Med. 2025;5:28. [DOI]
24. Huang L, Dong Y, Li J, Yang X, Li X, Wu J, et al. Epidermal Growth Factor Receptor (EGFR)-Targeting Peptides and Their Applications in Tumor Imaging Probe Construction: Current Advances and Future Perspectives. Biology. 2025;14:1011. [DOI] [PubMed] [PMC]
25. Bondarev N, Ivanenko K, Khabusheva E, Lebedev T, Manukhov I, Prassolov V. MGL S3 Chimeric Enzyme Drives Apoptotic Death of EGFR-Dependent Cancer Cells through ERK Downregulation. Int J Mol Sci. 2022;23:12807. [DOI] [PubMed] [PMC]
26. Bondarev NA, Bagaeva DF, Bazhenov SV, Buben MM, Bulushova NV, Ryzhykau YL, et al. Methionine gamma lyase fused with S3 domain VGF forms octamers and adheres to tumor cells via binding to EGFR. Biochem Biophys Res Commun. 2024;691:149319. [DOI] [PubMed]
27. Nguyen LT, Yang XZ, Du X, Wang JW, Zhang R, Zhao J, et al. Enhancing tumor-specific intracellular delivering efficiency of cell-penetrating peptide by fusion with a peptide targeting to EGFR. Amino Acids. 2015;47:997–1006. [DOI] [PubMed]
28. Kohen F, Gayer B, Kulik T, Frydman V, Nevo N, Katzburg S, et al. Synthesis and Evaluation of the Antiproliferative Activities of Derivatives of Carboxyalkyl Isoflavones linked to N-t-Boc-hexylenediamine. J Med Chem. 2007;50:6405–10. [DOI] [PubMed]
29. Kulikova VV, Morozova EA, Revtovich SV, Kotlov MI, Anufrieva NV, Bazhulina NP, et al. Gene cloning, characterization, and cytotoxic activity of methionine γ-lyase from *Clostridium novyi*. IUBMB Life. 2017;69:668–76. [DOI] [PubMed]
30. Crowley LC, Chojnowski G, Waterhouse NJ. Measuring the DNA Content of Cells in Apoptosis and at Different Cell-Cycle Stages by Propidium Iodide Staining and Flow Cytometry. Cold Spring Harb Protoc. 2016;2016:pdb.prot087247. [DOI] [PubMed]
31. Wei M, Wang R, Peng J, Li Z, Ali AR, Bian J, et al. The application prospects of amino acid deprivation for cancer therapy. Eur J Med Chem. 2026;308:118705. [DOI] [PubMed]
32. Garg P, Krishna M, Singhal SS. Small but mighty: Peptides as next-generation immunotargeting agents in gynecological cancers. Transl Oncol. 2026;67:102751. [DOI] [PubMed] [PMC]
33. Rodrigues Toledo C, Tantawy AA, Lima Fuscaldi L, Malavolta L, de Aguiar Ferreira C. EGFR- and Integrin αVβ3-Targeting Peptides as Potential Radiometal-Labeled Radiopharmaceuticals for Cancer Theranostics. Int J Mol Sci. 2024;25:8553. [DOI] [PubMed] [PMC]

34. Fekry M, Mazrouaa AM, Mohamed MG, Kishta MS, Mansour NA. The Comparison between Magnetite Nanoparticles Co-Precipitated by Different Bases and Their Effects on Human Cells. Int J Nanosci. 2021;20:2150021. [DOI]
35. Cell line – EGFR – The Human Protein Atlas [Internet]. The Human Protein Atlas; [cited 2026 Apr 15]. Available from: https://www.proteinatlas.org/ENSG00000146648-EGFR/cell+line#skin_cancer
36. Abo Qoura L, Babayeva G, Kolpaksidi AP, Pokrovsky VS. l-lysine α-oxidase encapsulation in red blood cells - Derived extracellular vesicles as biocompatible nanoplatform for cancer therapy. Biochem Biophys Res Commun. 2025;775:152130. [DOI] [PubMed]
37. Abo Qoura L, Morozova E, Ramaa CS, Pokrovsky VS. Smart nanocarriers for enzyme-activated prodrug therapy. J Drug Target. 2024;32:1029–51. [DOI] [PubMed]
38. Kishta MS, Hafez AM, Hydara T, Hamed Z, Bahr MM, Shamaa AA, et al. The transforming role of wharton's jelly mesenchymal stem cell-derived exosomes for diabetic foot ulcer healing: a randomized controlled clinical trial. Stem Cell Res Ther. 2025;16:559. [DOI] [PubMed] [PMC]
39. Zoheir KMA, Ali NI, Ashour AE, Kishta MS, Othman SI, Rudayni HA, et al. Lipoic acid improves wound healing through its immunomodulatory and anti-inflammatory effects in a diabetic mouse model. J Diabetes Metab Disord. 2025;24:56. [DOI] [PubMed] [PMC]